Analysis of Upsets and Failures Due to ESD by the FDTD-INBCs Method

Francescaromana Maradei and Marco Raugi

***Abstract*—In this paper, a finite-difference time-domain (FDTD) model of an electrostatic discharge (ESD) event is developed. Analytical expressions for the field radiated during the ESD discharge phase have been determined to test the FDTD model of the strike arc. In order to take into account the electromagnetic field penetration through shielding structures, the conductive panels are efficiently modeled in the FDTD by the impedance network boundary conditions (INBCs). The FDTD-INBCs method avoids the huge amount of cells needed to model accurately the penetration in the traditional FDTD algorithm based on the utilization of the regular Yee grid. The method is applied to the analysis of ESD events in some configurations.**

***Index Terms*—Electrostatic discharge, finite-difference time-domain method, impedance network boundary conditions.**

I. Introduction

CURRENTS and voltages induced in the enclosure of electronic apparata due to an electrostatic discharge (ESD) may produce damage, failures, or upsets. Thus, devices that operate in an industrial environment, where there is a high probability of ESD events on the enclosure of the electric and electronic apparata, must comply with immunity standards and tests. To get through the required tests, a suitable design of these devices is needed. Because of the variety and complexity of the devices which are victims of ESD, numerical simulation of ESD electromagnetic phenomena is required for a proper design in order to limit the probability of upset and damage.

The ESD effects are usually observed by separating the so-called "indirect" effects of the radiated fields during the strike arc, and the "direct" effects during the current conduction phase. Indirect effects due to the radiated fields during the arc discharge, represented by the induced voltages and currents in neighboring devices, are usually evaluated assuming the enclosures as perfectly conductive so that the electromagnetic interference is caused by the fields through the apertures [1], [2]. Direct effects are due to the direct injection of current in a device victim of an ESD and they are usually modeled assuming a known current waveform injected between two points of the victim device [3], [4]. These effects are actually coupled and, therefore, a complete model of the ESD phenomenon has to be considered to determine its effect on the equipment directly affected by the discharge current. Furthermore, if the enclosures are realized with low conductive materials or with plastics coated by conductive films, the penetration through the walls could be considerable, even in the case of indirect ESD events, and has to be taken into account.

In this paper, a numerical model based on a finite-difference time-domain method (FDTD) formulation with impedance network boundary conditions (INBCs) is presented. The INBCs [5], [6] are applied on the surface of conductive panels and take into account the field penetration through the panels, avoiding the large space discretazion required by standard FDTD method. The model of the ESD discharge in the FDTD procedure is discussed and validated by comparing the numerical results with those achieved by a filamentary arc analytical approach.

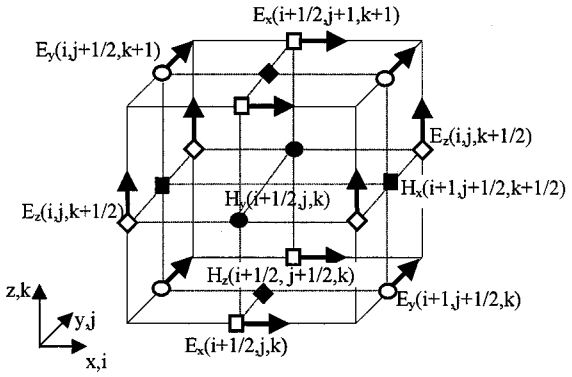

Fig. 1. Position of the electric and magnetic field components in the basic Yee cell.

II. FDTD Method

The FDTD method is a very popular time-domain technique because of the simplicity of the explicit solution scheme and the capability in modeling complex configurations.

The method is based on the numerical solution of the time-domain Maxwell's curl equations

$$\nabla \times \mathbf{E}(\mathbf{r}, t) = -\mu_0 \frac{\partial \mathbf{H}(\mathbf{r}, t)}{\partial t} \tag{1a}$$

$$\nabla \times \mathbf{H}(\mathbf{r}, t) = \varepsilon_0 \frac{\partial \mathbf{E}(\mathbf{r}, t)}{\partial t} + \mathbf{J}(\mathbf{r}, t) \tag{1b}$$

where $\mathbf{E}(\mathbf{r}, t)$ and $\mathbf{H}(\mathbf{r}, t)$ are the electric and magnetic fields, respectively, $\mathbf{J}(\mathbf{r}, t)$ the current density, μ_0 and ε_0 the free-space permeability and permittivity, respectively, and $\mathbf{r}$ the position vector.

Paper MSDAD-A 02–11, presented at the 2000 Industry Applications Society Annual Meeting, Rome, Italy, October 8–12, and approved for publication in the IEEE TRANSACTIONS ON INDUSTRY APPLICATIONS by the Electrostatic Processes Committee of the IEEE Industry Applications Society. Manuscript submitted for review October 15, 2000 and released for publication May 2, 2002.

F. Maradei is with the Department of Electrical Engineering, University of Rome "La Sapienza," I-00184 Rome, Italy (e-mail: maradei @elettrica.ing.uniroma1.it).

M. Raugi is with the Department of Electrical Systems and Automation, University of Pisa, I-56126 Pisa, Italy (e-mail: raugi@dsea.unipi.it).

Publisher Item Identifier 10.1109/TIA.2002.800775.

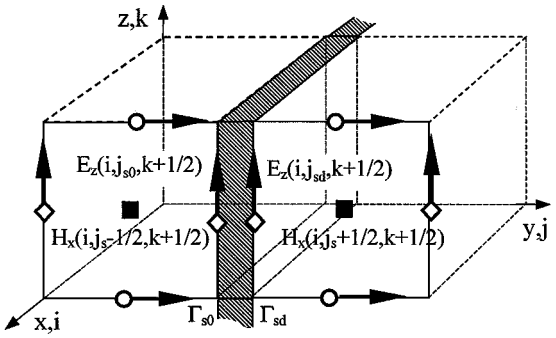

Fig. 2. FDTD cells in proximity of the thin conductive panel.

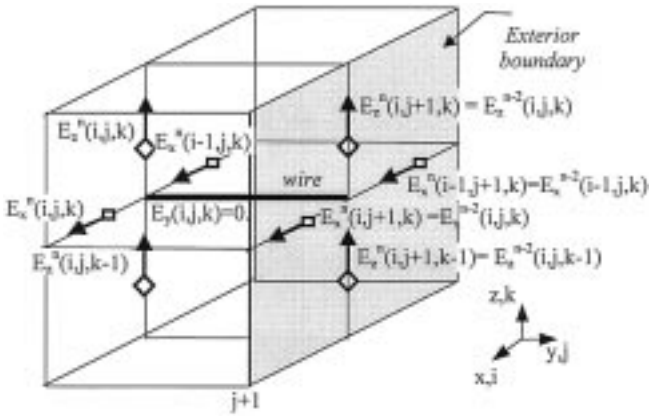

Fig. 3. Exact ABCs used to model a perfect wire conductor crossing the exterior boundary.

In the FDTD method the computational domain is discretized by cubic cells and on each cell the field components are positioned as illustrated in Fig. 1. Approximating the spatial derivatives in (1) on the Yee grid by central finite differences, and adopting the *leap-frog* scheme for the time derivatives, the following expressions to update the magnetic and electric field x components are derived [7], [8]:

$$\begin{aligned} H_x^{n+1/2}&(i,\, j+1/2,\, k+1/2) \\ &= H_x^{n-1/2}(i,\, j+1/2,\, k+1/2) \\ &\quad - \frac{\Delta t}{\mu_0 \Delta}\left[E_z^n(i,\, j+1,\, k+1/2) - E_z^n(i,\, j,\, k+1/2)\right] \\ &\quad + \frac{\Delta t}{\mu_0 \Delta}\left[E_y^n(i,\, j+1/2,\, k) - E_y^n(i,\, j+1/2,\, k+1)\right] \end{aligned} \tag{2a}$$

$$\begin{aligned} E_x^{n+1}&(i+1/2,\, j,\, k) \\ &= E_x^{n-1}(i+1/2,\, j,\, k) - \frac{\Delta t}{\varepsilon_0} J_x^{n+1/2}(i+1/2,\, j,\, k) \\ &\quad + \frac{\Delta t}{\varepsilon_0 \Delta}\Big[H_z^{n-1/2}(i+1/2,\, j+1/2,\, k) \\ &\qquad - H_z^{n-1/2}(i+1/2,\, j-1/2,\, k)\Big] \\ &\quad - \frac{\Delta t}{\varepsilon_0 \Delta}\Big[H_y^{n-1/2}(i+1/2,\, j,\, k+1/2) \\ &\qquad - H_y^{n-1/2}(i+1/2,\, j,\, k-1/2)\Big] \end{aligned} \tag{2b}$$

where the superscripts $(n \pm 1/2)$ and n refer to the time instants $t = (n \pm 1/2)\Delta t$ and $t = n\Delta t$, respectively, $\Delta = \Delta x = \Delta y = \Delta z$ is the cell dimension, and the indexes in parenthesis represent the spatial position of the field components according to the notation adopted in Fig. 1. The expressions for the calculation of the other field components can be easily derived. The FDTD method is a conditionally stable method; therefore, to assure numerical stability the Courant stability condition must be satisfied [7]. A good choice for the time step is $\Delta t = \Delta/(2c)$ where c is the free-space propagation velocity.

A. Model of Conductive Panels by INBCs

The interaction of the electromagnetic field with shielding panels is modeled by suitable boundary conditions on the shield surface. If the shield is made of perfectly conductive material, the boundary conditions require $\mathbf{E}\cdot\boldsymbol{\tau} = 0$, with $\boldsymbol{\tau}$ the unit vector tangent to the panel walls. In some practical cases, the panels of the enclosure containing electronic circuits and devices are realized with low-conductive materials or with plastics coated by conductive films, and the penetration through the walls could be considerable. In order to take into account the electromagnetic field penetration through the shielding panels, INBCs derived from the shielding theory [9] have been developed and successfully implemented in a three–dimensional (3-D) FDTD code [5], [6]. Let us consider a shield panel normal to the y axis and positioned at $j = j_s$. The INBCs for the field components $E_z(i,\, j_{s0},\, k)$ and $E_z(i,\, j_{sd},\, k)$ on the two panel surfaces Γ_{s0} and Γ_{sd} shown in Fig. 2 can be written as

$$\begin{aligned} E_z^n&(i,\, j_{s0},\, k+1/2) \\ &= \left[\zeta_0(t) * \frac{\partial H_x(i,\, j_s - 1/2,\, k+1/2,\, t)}{\partial t}\right]_{n\Delta t} \\ &\quad - \left[\zeta_m(t) * \frac{\partial H_x(i,\, j_s + 1/2,\, k+1/2,\, t)}{\partial t}\right]_{n\Delta t} \end{aligned} \tag{3a}$$

$$\begin{aligned} E_z^n&(i,\, j_{sd},\, k+1/2) \\ &= \left[\zeta_m(t) * \frac{\partial H_x(i,\, j_s - 1/2,\, k+1/2,\, t)}{\partial t}\right]_{n\Delta t} \\ &\quad - \left[\zeta_0(t) * \frac{\partial H_x(i,\, j_s + 1/2,\, k+1/2,\, t)}{\partial t}\right]_{n\Delta t} \end{aligned} \tag{3b}$$

where the symbol $*$ represents the convolution integral, and $\zeta_0(t)$ and $\zeta_m(t)$ are the transient impedances of the panel [5], [6]. The explicit expressions to update the magnetic field in the two cells adjacent to the shield and the validation of the proposed INBCs can be found in [5] and [6].

B. Model of the ESD Discharge Path

The ESD current $i_{\rm esd}(t)$ associated with an ESD event is supposed to be known either from measurements or by using the waveforms reported in the immunity standards [10]. The discharge path is simulated by a known current density in one FDTD cell that simulates the ESD ionized channel. This model is based on the assumption that the ESD current is uniformly distributed in the channel so that the current density is $J = i_{\rm esd}(t)/\Delta^2$. The effects of the ESD channel approximation will be evaluated comparing the numerical radiated fields with the

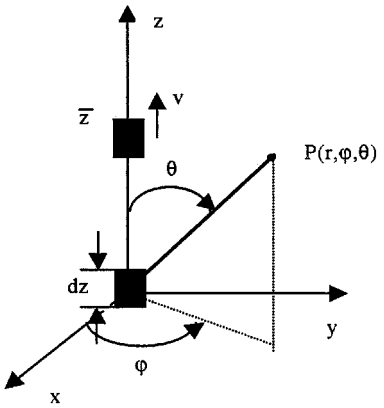

Fig. 4. Configuration of a current element.

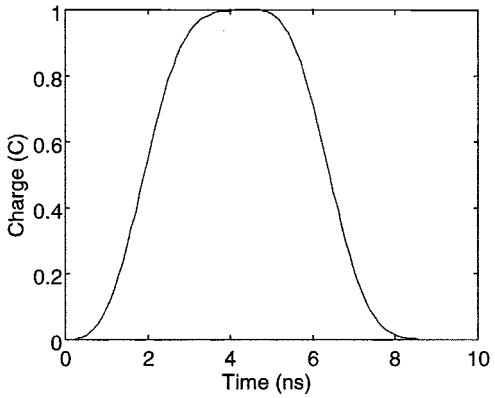

Fig. 5. Charge waveform used to compare the FDTD result with the analytical solution.

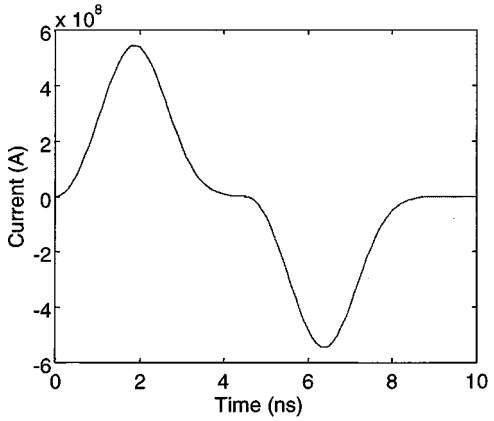

Fig. 6. Current waveform used to compare the FDTD result with the analytical solution.

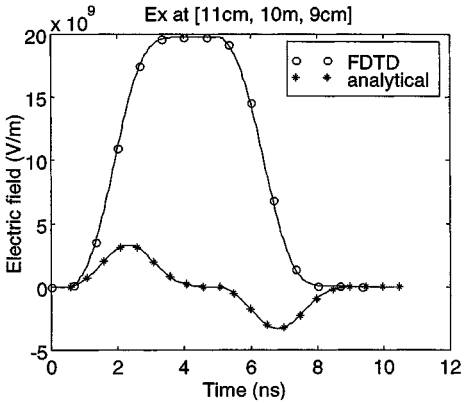

Fig. 7. Comparison between the FDTD result and the analytical solution.

fields produced by the filamentary model described in the next section.

In the physics of the ESD event, there is an initial accumulation of electrical charges localized on two electrodes that yields a breakdown voltage between the electrodes and starts the discharge phase. Therefore, the ESD event is characterized by a nonzero distribution of the electric field and a zero distribution of the magnetic field at the time instant $t = 0$, which represent the starting instant of the discharge phase. The value of the initial charge can be derived from the known ESD current and produces a static distribution of the electric field, which can be calculated as proposed in [18]. The nonzero values of the electric field affect the electromagnetic field solution especially in the proximity of the discharge path, while they have a very low influence in the remaining part of the domain.

C. Model of the Grounding System

In practical configurations the object struck by the ESD event is provided by one or more grounding connections. Since the dimensions of the grounding system are quite large (i.e., the grounding conductors can run for long distances, and the ground reference plane can be very large), it is not possible to model the whole grounding system in the FDTD computational domain. In order to overcome this problem, the domain is reduced to the region of space affected by the ESD event. In this case, the region includes some wire conductors that cross the boundary of the computational domain.

The wire conductors are modeled in the FDTD code as perfect conductors and the electric field tangent to the wire is set to zero. The radiated field is absorbed on the exterior boundary by applying a second-order Mur absorbing boundary conditions (ABCs) [11] suitably modified in the proximity of the wire conductors. Indeed, in order to avoid any reflection of the current flowing through the wire conductors when passing across the boundary, exact one-dimensional truncation lattice conditions are applied [12]. Let us consider the wire conductor parallel to the y axis and crossing the boundary plane $j = j+1$ as shown in Fig. 3. The exact one-dimensional truncation lattice conditions are

$$E_x^n(i-1,\, j+1,\, k) = E_x^{n-2}(i-1,\, j,\, k) \tag{4a}$$

$$E_x^n(i,\, j+1,\, k) = E_x^{n-2}(i,\, j,\, k) \tag{4b}$$

$$E_z^n(i,\, j+1,\, k-1) = E_z^{n-2}(i,\, j,\, k-1) \tag{4c}$$

$$E_z^n(i,\, j+1,\, k) = E_z^{n-2}(i,\, j,\, k). \tag{4d}$$

III. Filamentary Arc Model

A model that assumes a filamentary discharge path for the ESD current has also been developed. This model is obtained by models of electrical discharges in short air gaps [13]–[15] and gives analytical expressions for the radiated fields. Indeed, in electronic devices and industrial environments, ESDs are more

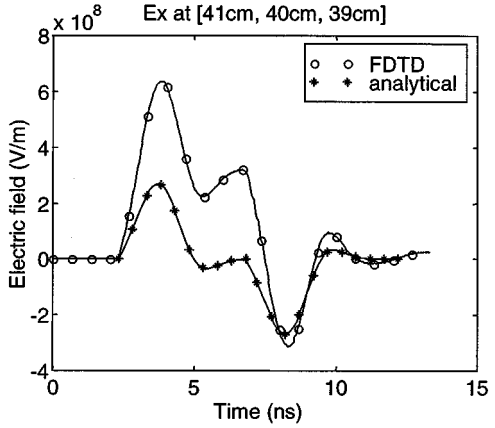

Fig. 8. Comparison between the FDTD result and the analytical solution.

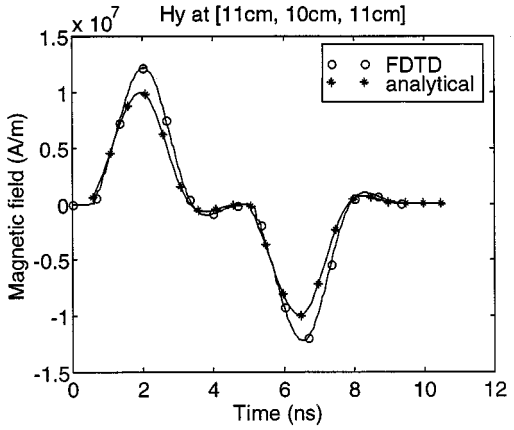

Fig. 9. Comparison between the FDTD result and the analytical solution.

frequently due to proximity effects; the physics of electric discharges in short air gaps is characterized by shorter duration and different parameters with respect to long air sparks that are essentially related to the lightning phenomenon. We have assumed that owing to a charge accumulation on the device (negative point) that faces a charge accumulation on a neighbor surface (positive point), the onset voltage is reached and the discharge occurs. The discharge can be modeled by two phases characterized by the primary streamers propagation and by the current conduction in the ionized channel, respectively.

A. Primary Streamers Propagation

The primary streamers propagation has been modeled by means of a spatial growing column of current with a positive charge with its head at $z = \overline{z}$. The column tip is supposed to propagate with a constant average velocity v, and the current from the positive rail to the column tip has been set constant both with time and with position. Furthermore, during the streamers propagation the accumulated charges on the surfaces remain present. The electromagnetic field during this phase has been analytically calculated and reported in (5) and (6) in spherical coordinates.

We refer to the geometry of Fig. 4 and we determine the electromagnetic fields dE and dB generated by a filamentary element of height dz, placed at the origin, directed along the z axis and with a current $i(t)$ in it. Assuming a step current $i(t)$ in the element, we evaluate the electromagnetic fields due to a current

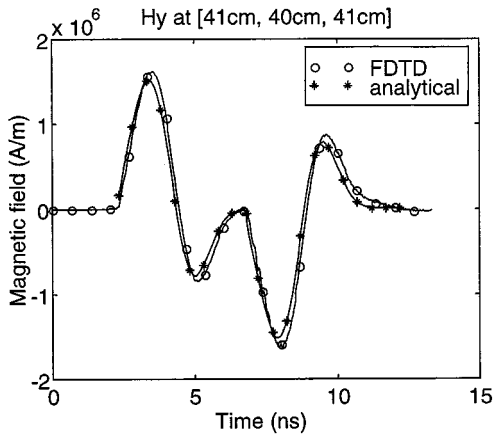

Fig. 10. Comparison between the FDTD result and the analytical solution.

column of height h by $E = \int_0^h dE$ and $B = \int_0^h dB$ obtaining (5) and (6), as shown at the bottom of the next page.

B. Current Conduction in the Ionized Channel

The current conduction in the channel occurs when the spatial growing column between $\overline{z}_1$ and $\overline{z}_2$ reaches the negative point, and the gap, considered as a short circuit, is crossed by the current. The waveform of this current corresponds to the charge flow through the ionized gap needed to extinguish the existing charges on the negative and positive points during the streamers propagation.

The analytical expressions of the electromagnetic field, referred again to Fig. 4, are as shown in (7) and (8), at the bottom of the next page.

IV. Applications

A. Radiated Field: Analytical versus FDTD Results

The actual ESD current discharge path can be considered as a filamentary path. To test the validity of the FDTD model, where the ESD current is considered as distributed into a FD cell of the discretized domain, we compared the numerical radiated fields with the analytical ones.

To test only the fields radiated by the ESD current we consider an isolated current element in free space. The computational domain of 1 m $\times$ 1 m $\times$ 1 m is discretized by cells of dimension $\Delta = 2$ cm, and $\Delta t = 33.33$ ps is adopted. The current element oriented along the z axis is positioned in the center of the domain.

For simplicity, to avoid the static distribution of the electric field at the time instant $t = 0$, the charge shown in Fig. 5 and the corresponding current shown in Fig. 6 have been assumed.

The isolated current element considered in the FDTD simulation corresponds to a dipole having a charge $Q = \int i(t)\,dt$ on either pole. In the source proximity, the electric field is dominated by the static charge field as can be seen from Figs. 7 and 8 where the FDTD fields are similar to the charge waveform. In actual ESD events, the system cannot hold a static charge and, therefore, this phenomenon affects only the isolated dipole configuration and does not appear in practical configurations. Indeed, the analytical electric fields shown in Figs. 7 and 8 are similar to the current waveform. Thus, the actual comparison

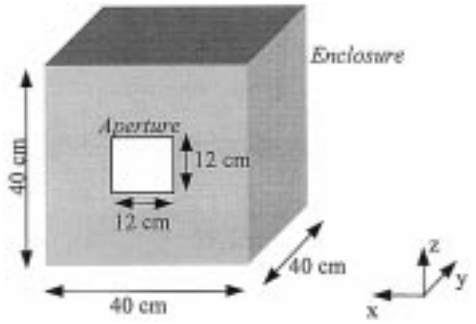

Fig. 11. Configuration of the enclosure with aperture adopted in the simulations.

between the models has to be carried out by controlling the magnetic fields which are not affected by this phenomenon.

The main influence of the ESD radiated fields are in the proximity of the ESD event, hence, we concentrate our analysis in a box 40 cm $\times$ 40 cm $\times$ 40 cm around the discharge. The y-component magnetic field obtained by the FDTD simulation and by the filamentary model at about 10 cm and 40 cm from the discharge are shown in Figs. 9 and 10. It should be noted that the discrepancies between the two solutions are significant (about 10% relative error at the peak value) only in the proximity of the ESD event (see Fig. 9), where the finite dimension of the FD discharge channel cannot represent the actual filamentary ones.

The discrepancies diminish as the distance from the source increases, as shown in Fig. 10 (about 3% relative error at the peak value), and completely disappear when the distance from the source is much greater than the FD cell dimension [16]. Thus,

$$\begin{bmatrix} E_{i,r} \\ E_{i,\varphi} \\ E_{i,\theta} \end{bmatrix} = \frac{I}{4\pi\varepsilon_0} v \left(vc(\overline{z} - r\cos\theta) + c^2(r^2 + \overline{z}^2 - 2r\overline{z}\cos\theta)^{1/2} \right)^{-1} \begin{bmatrix} -\cos\theta \\ 0 \\ \sin\theta \end{bmatrix}_{\overline{z}(r^2+\overline{z}^2-2r\overline{z}\cos\theta)^{1/2}=c(t-(\overline{z}/v))} \tag{5}$$

$$\begin{bmatrix} B_{i,r} \\ B_{i,\varphi} \\ B_{i,\theta} \end{bmatrix} = \mu_0 \frac{Ir\sin\theta}{4\pi} v \left(vc(\overline{z} - r\cos\theta) + c^2(r^2 + \overline{z}^2 - 2r\overline{z}\cos\theta)^{1/2} \right)^{-1} \cdot \left[\int_0^{\overline{z}} \frac{\begin{matrix} 0 \\ dz^* \\ 0 \end{matrix}}{(r^2 + z^{*2} - 2rz^*\cos\theta)^{3/2}} + v \left(v(r^2 + \overline{z}^2 - 2r\overline{z}\cos\theta)^{1/2} + (\overline{z} - r\cos\theta) \right. \right. \left. \left. + c(r^2 + \overline{z}^2 - 2r\overline{z}\cos\theta) \right)^{-1} \right]_{\overline{z}(r^2+\overline{z}^2-2r\overline{z}\cos\theta)^{1/2}=c(t-(\overline{z}/v))} \tag{6}$$

$$\begin{bmatrix} E_{i,r} \\ E_{i,\varphi} \\ E_{i,\theta} \end{bmatrix} = \frac{I}{4\pi\varepsilon_0} \begin{bmatrix} \dfrac{\cos\theta}{c(\overline{z}_1 - r\cos\theta)} - \dfrac{\cos\theta}{c(\overline{z}_2 - r\cos\theta)} \\ 0 \\ -\dfrac{\sin\theta}{c(\overline{z}_1 - r\cos\theta)} + \dfrac{\sin\theta}{c(\overline{z}_2 - r\cos\theta)} \end{bmatrix}_{\substack{\overline{z}_2(r^2+\overline{z}^2-2r\overline{z}_2\cos\theta)^{1/2}=ct \\ \overline{z}_1(r^2+\overline{z}^2-2r\overline{z}_1\cos\theta)^{1/2}=ct}} \tag{7}$$

$$\begin{bmatrix} B_{i,r} \\ B_{i,\varphi} \\ B_{i,\theta} \end{bmatrix} = \mu_0 \frac{Ir\sin\theta}{4\pi} \left[\int_{\overline{z}_1}^{\overline{z}_2} \frac{\begin{matrix} 0 \\ dz^* \\ 0 \end{matrix}}{(r^2 + z^{*2} - 2rz^*\cos\theta)^{3/2}} - \frac{\begin{matrix} 0 \\ 1 \\ 0 \end{matrix}}{(r^2 + \overline{z}_1^2 - 2r\overline{z}_1\cos\theta)^{1/2}(\overline{z}_1 - r\cos\theta)} \right. \left. + \frac{\begin{matrix} 0 \\ 1 \\ 0 \end{matrix}}{(r^2 + \overline{z}_2^2 - 2r\overline{z}_1\cos\theta)^{1/2}(\overline{z}_2 - r\cos\theta)} \right]_{\substack{\overline{z}_2(r^2+\overline{z}^2-2r\overline{z}_2\cos\theta)^{1/2}=ct \\ \overline{z}_1(r^2+\overline{z}^2-2r\overline{z}_1\cos\theta)^{1/2}=ct}} \tag{8}$$

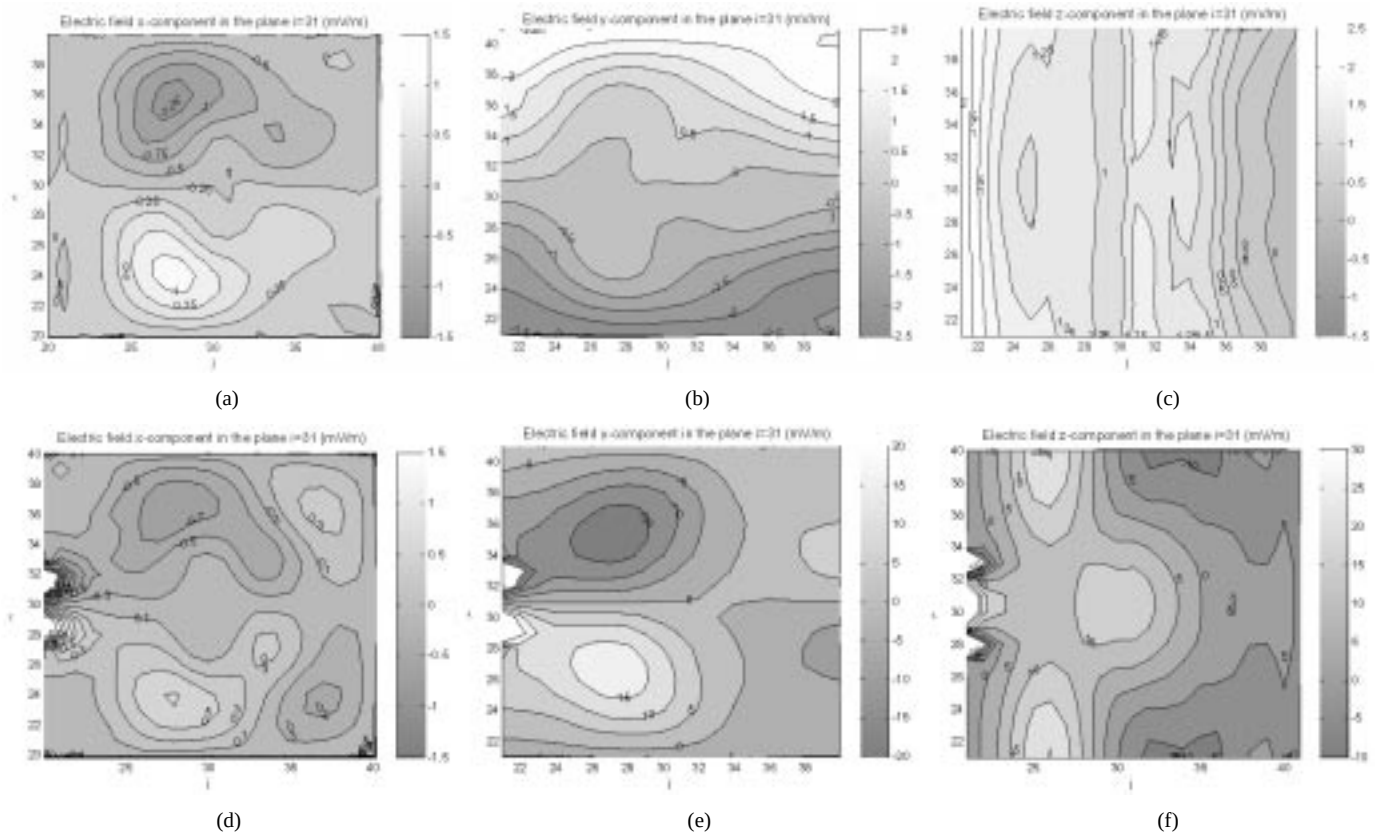

(a) (b) (c)

(d) (e) (f)

Fig. 12. Maps of the electric field components in the pane $i = 31$ (i.e., $x = 0.6$ m) after 140 iterations. (a)–(c) Inside the closed box. (d)–(f) Inside the box with aperture.

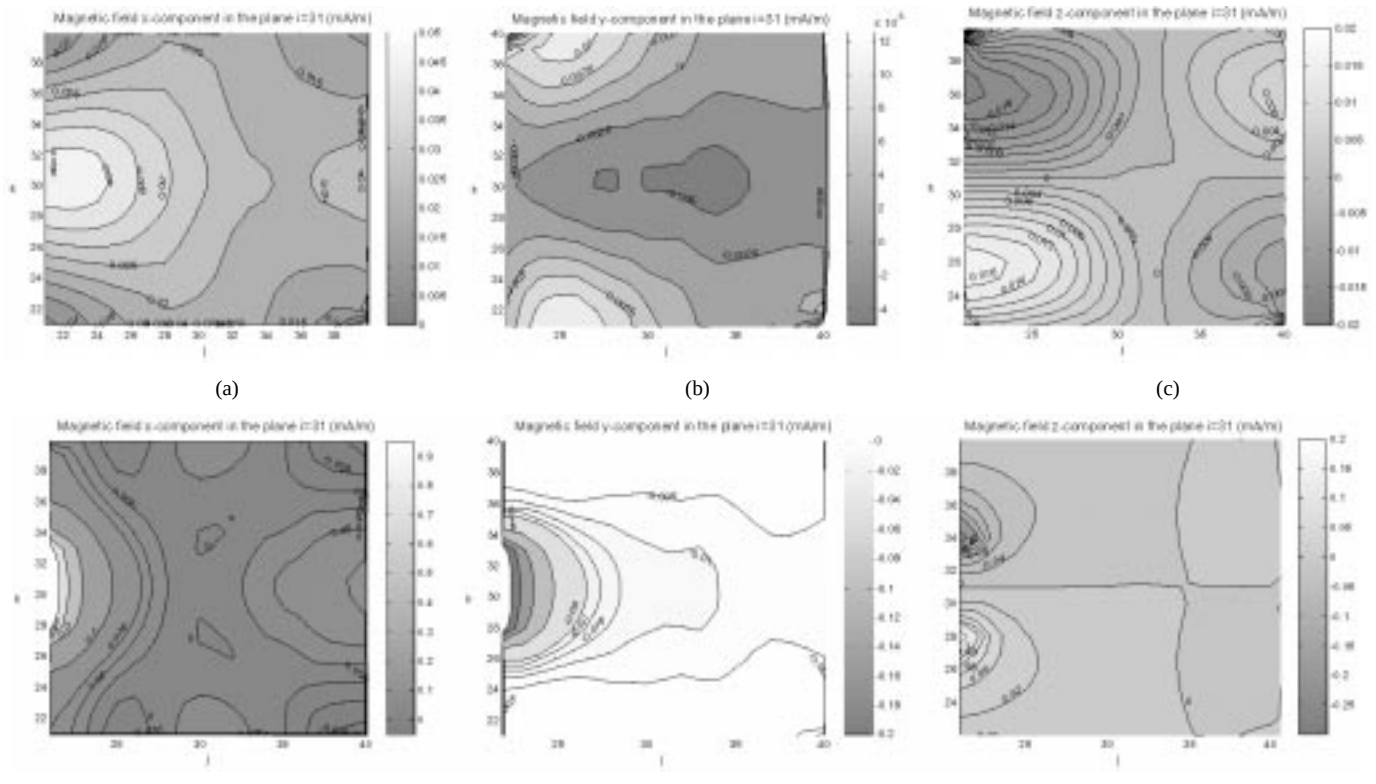

(a) (b) (c)

(d) (e) (f)

Fig. 13. Maps of the magnetic field components in the plane $i = 31$ (i.e., $x = 0.6$ m) after 140 iterations. (a)–(c) Inside the closed box. (d)–(f) Inside the box with aperture.

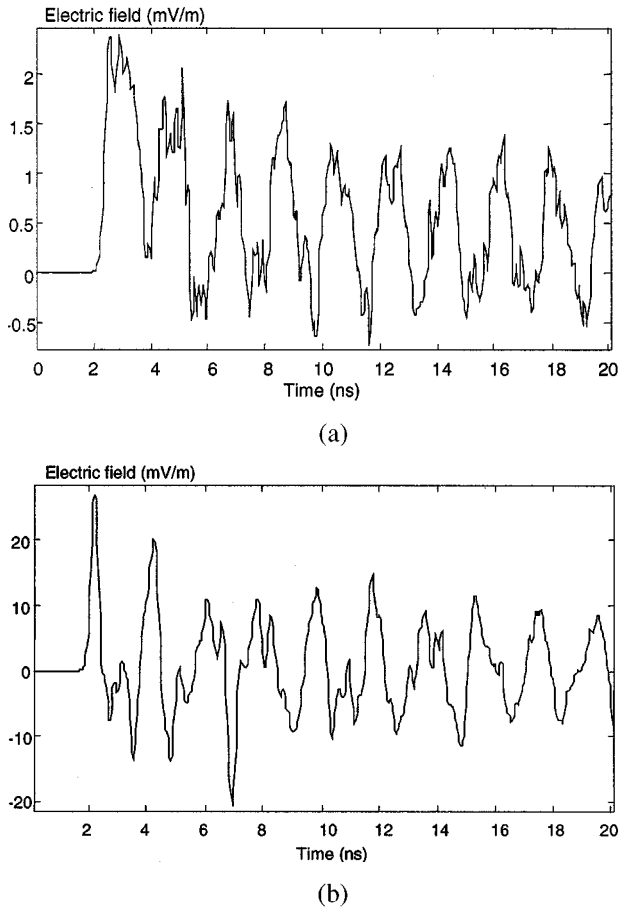

Fig. 14. Transient behavior of the z component of the electric field $E_z(31,\ 31,\ 31.5) = E_z(x = 0.6\,\text{m},\ y = 0.6\,\text{m},\ z = 0.61\,\text{m})$ at (a) the central point of the closed box and of (b) the box with aperture.

the FDTD model gives an acceptable overall approximation of the filament model of an ESD discharge.

B. Numerical Simulations

The system under investigation is an enclosure of dimensions 40 cm × 40 cm × 40 cm. The enclosure walls have thickness $d = 1$ mm and conductivity $\sigma = 1000$ S/m. It should be noted that this value of conductivity is suitable to model materials such as composites [19]. Initially, in order focus the attention only on the electromagnetic penetration through the conductive walls, an enclosure with no apertures has been considered.

Then, an aperture of dimensions 12 cm × 12 cm on one side of the enclosure has been introduced, as shown in Fig. 11. The computational domain of dimension 1.2 m × 1.2 m × 1.2 m is discretized by cells of size $\Delta = 2$ cm, and $\Delta t = 33.33$ ps is adopted. The box is placed in the center of the domain.

The test configurations have been first analyzed assuming that the ESD event does not occur in proximity of the enclosure. In this case, the electromagnetic field that illuminates the box can be assumed as a plane-wave field. The box is, therefore, excited by a plane wave propagating in the y direction (i.e., azimuth angle $\phi = 90°$ and elevation angle $\theta = 90°$), and characterized by an incident electric field $E_z^i(t) = \exp(-5 \cdot 10^7 t) - \exp(-10^9 t)$ V/m having a peak value of about 1 V/m.

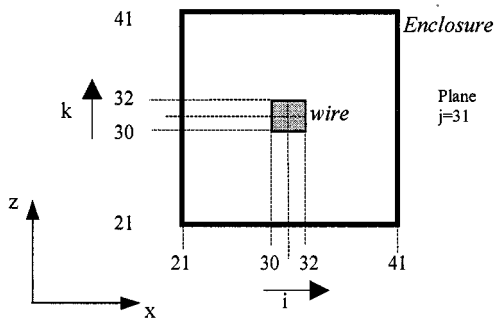

Fig. 15. Configuration of a square loop placed inside the enclosure in the plane $j = 31$ (i.e., $y = 0.6$ m).

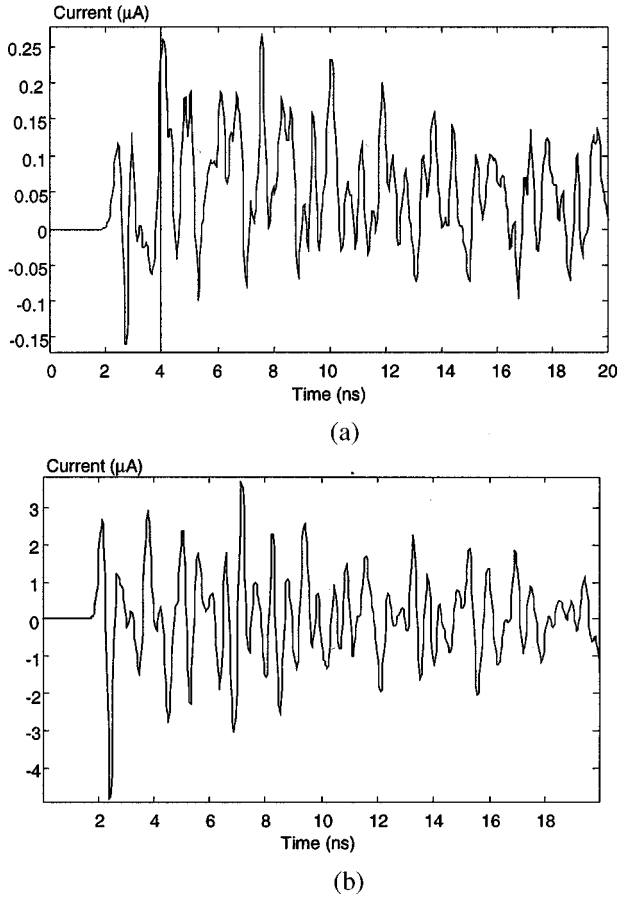

Fig. 16. Transient behavior of the current induced in a square loop of edge 4 cm positioned in the center of (a) the closed box and of (b) the box with aperture in the plane $j = 31$.

The maps of the electric and magnetic field components inside the enclosure after 140 iterations for the closed box and for the enclosure with aperture are shown in Figs. 12 and 13. The figures show that the E_z and H_x components dominate the other components either with or without apertures. The figures show that, without the aperture, the fields inside the box are about one order of magnitude lower than when the aperture is present. Nevertheless, the field penetration is not negligible, and its influence can induce upsets inside the box.

The transient behavior of the z component of the electric field in the central point of the box, i.e., $E_z(31,\ 31,\ 31.5) = E_z(x = 0.6\,\text{m},\ y = 0.6\,\text{m},\ z = 0.61\,\text{m})$, for the two boxes considered

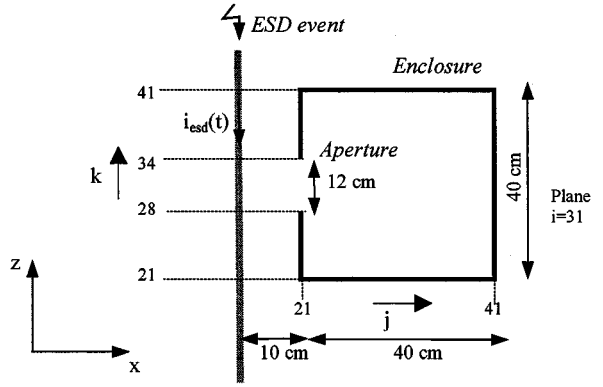

Fig. 17. Configuration of the enclosure in the proximity of a wire conductor in the plane $i = 31$ (i.e., $x = 0.6$ m).

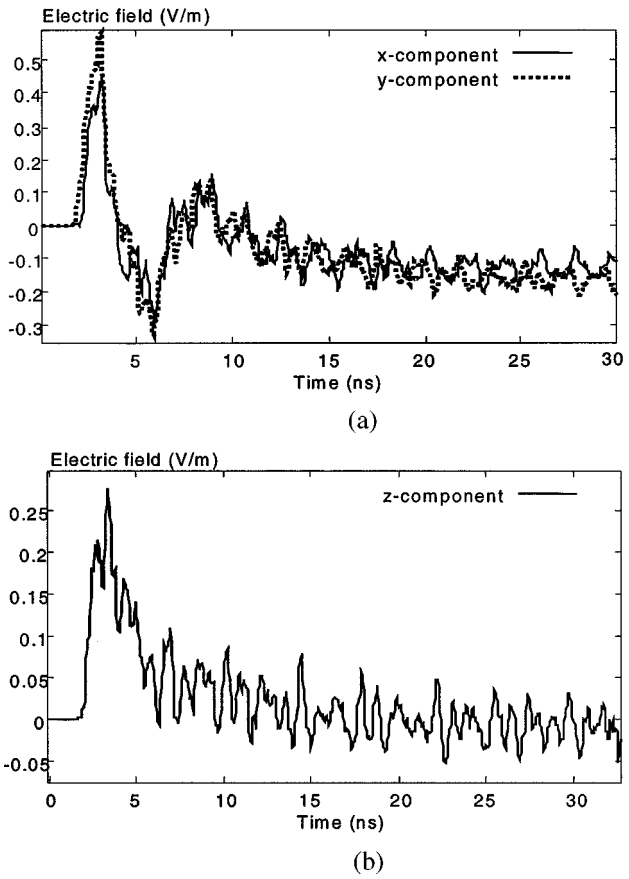

Fig. 18. Transient behavior of the electric field at the central point (i.e., cell $i = 31, j = 31, k = 31$) of the closed box. (a) x and y components. (b) z component.

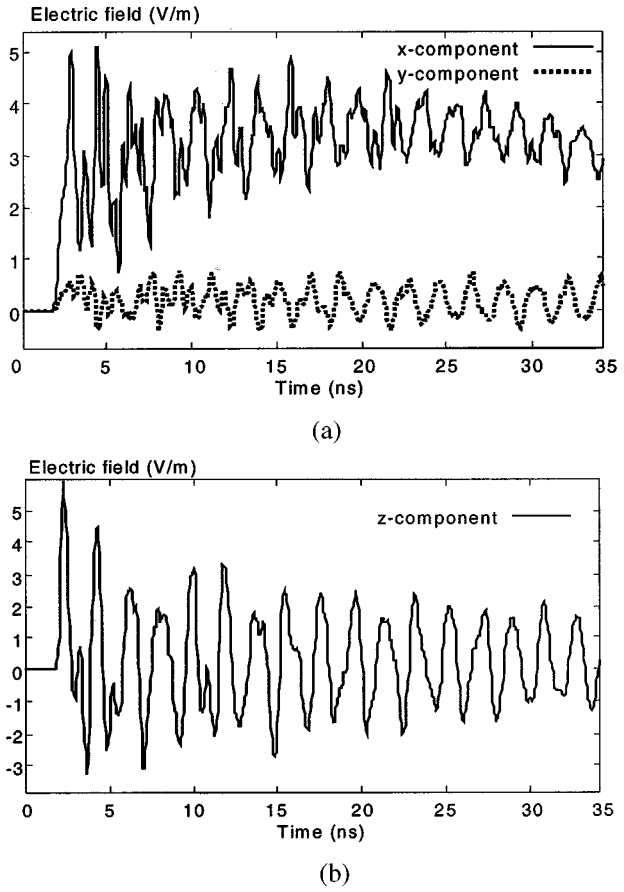

Fig. 19. Transient behavior of the electric field at the central point (i.e., cell $i = 31, j = 31, k = 31$) of the box with the aperture. (a) x and y components. (b) z component.

are shown in Fig. 14. The waveforms show a high harmonic content because the enclosure acts as a resonant cavity.

To evaluate the induced effects inside the box a square loop of edge 4 cm is introduced in the center of the enclosure in the plane $j = 31$ as shown in Fig. 15.

The current induced in the loop placed inside the closed box and inside the box with aperture is shown in Fig. 16. Comparison of the results obtained for the two configurations confirms that the fields inside the enclosure and therefore the induced current in the square loop are greater in the case of the box with the aperture since the field penetrating through the aperture is dominant.

Currents of a few tens of milliamperes can induce upsets in boards placed inside the enclosures. Therefore, incident fields comparable with the measured ESD fields [17], which can reach hundreds of V/m, can induce upsets inside the enclosures either with and without apertures realized with low conductive materials.

In the second application, the enclosure under investigation is assumed to be placed in the proximity of a wire conductor through which the current produced by an ESD event flows. This case represents a situation where the enclosure is illuminated by a near field source. The wire is assumed to cross the computational boundary and reach a ground plane outside the boundary as shown in Section II-C. The simulation is performed assuming that the wire conductor is parallel to the z axis and placed at a distance $d = 10$ cm from the box face, $j = 21$ (i.e., $y = 0.4$ m) in the plane $i = 31$ (i.e., $x = 0.6$ m) as shown in Fig. 17. The adopted ESD current is the same as for the plane wave $i_{\rm esd}(t) = \exp(-5 \cdot 10^7 t) - \exp(-10^9 t)$ A and has a peak value of about 1 A.

The transient behavior of the electric field components in the cell $i = 31$, $j = 31$, and $k = 31$, obtained for the closed box and for the box with the aperture are shown in Figs. 18 and 19.

The figures show that, in this case, the field components have similar amplitudes. It should be noted that the effects of the field penetration through the aperture are evident only on the x and z components of the electric field.

The amplitude of the induced fields in this case obviously depends on the distance between the wire and the box and on the amplitude of the ESD current which is typically of the order of tens of amperes [17]. Furthermore, for near field sources, the field components have nearly the same amplitude and, therefore, it can be expected that the induced effects could be significant for any orientation of the loop.

V. Conclusions

In this paper, an FDTD-INBCs model of an ESD event has been developed. The approximation of the radiated fields due to an ESD discharge considering the channel as an FD cell has been tested by comparison with the fields of a filamentary arc model, and a satisfactory agreement has been obtained.

The numerical model applied to practical configurations has highlighted the fact that the penetration of the fields cannot be neglected when the conductivity of the enclosures is relatively low, as often happens in practical apparata.

References

[1] P. Shubitidze, R. Jobava, R. Zaridze, D. Karkashadze, R. Beria, D. Pommerenke, and S. Frei, "FDTD method in problems of penetration of transient fields of electrostatic discharge into a cavity," in *Proc. VII Conf. Mathematical Methods in Electromagnetic Theory*, Kharkov, Ukraine, 1998, pp. 327–329.

[2] G. Cerri, R. De Leo, V. M. Primiani, and A. Venturi, "An efficient analysis of EM fields into shielded enclosures excited by ESD through rectangular slots," in *Proc. Int. Symp. Electromagnetic Compatibility—EMC'94 ROMA*, Rome, Italy, Sept. 13–16, 1994, pp. 853–858.

[3] M. Angeli, E. Cardelli, M. Raugi, and B. Tellini, "Computer simulation of the interferences produced by ESD via a differential and an integral method," in *Proc. Int. Symp. Electromagnetic Compatibility—EMC'98 ROMA*, Rome, Italy, Sept. 14–18, 1998, pp. 658–663.

[4] A. Aiello, R. De Leo, M. Trighetti, and G. Tribellini, "A theoretical model for thin shield effectiveness against ESD problems," in *Proc. Int. Symp. Electromagnetic Compatibility—EMC'96 ROMA*, Rome, Italy, Sept. 17–20, 1996, pp. 584–589.

[5] M. Feliziani, F. Maradei, and G. Tribellini, "Field analysis of penetrable conductive shields by the finite-difference time-domain method with impedance network boundary conditions (INBC's)," *IEEE Trans. Electromagn. Compat.*, vol. 41, pp. 207–319, Nov. 1999.

[6] M. Feliziani and F. Maradei, "Finite-difference time-domain modeling of thin shields," *IEEE Trans. Magn.*, vol. 36, pp. 848–851, July 2000.

[7] K. S. Yee, "Numerical solution of initial boundary value problems involving Maxwell's equations in isotropic media," *IEEE Trans. Antennas Propagat.*, vol. 14, pp. 302–307, May 1966.

[8] K. S. Kunz and J. Luebbers, *The Finite-Difference Time-Domain Method for Electromagnetics*. Boca Raton, FL: CRC Press, 1993.

[9] R. B. Schulz, V. C. Plantz, and D. R. Brush, "Shielding theory and practice," *IEEE Trans. Electromagn. Compat.*, vol. 30, pp. 187–201, Aug. 1988.

[10] *Electromagnetic Compatibility (EMC), Part 4: Testing and Measurement Techniques—Section 2: Electrostatic Discharge Immunity Test*, CEI-EN Pub. 61000-4-2.

[11] G. Mur, "Absorbing boundary conditions for the finite-difference approximation of the time domain electromagnetic field equations," *IEEE Trans. Electromagn. Compat.*, vol. 23, pp. 377–382, Nov. 1981.

[12] A. Taflove and M. E. Brodwin, "Numerical solution of steady-state electromagnetic problems using the time-dependent Maxwell's equations," *IEEE Trans. Microwave Theory Tech.*, vol. 23, pp. 623–630, Aug. 1975.

[13] G. Baldo, "Basic aspects of the physics concerning the development of long sparks in air," in *Proc. IEEE-PES Summer Meeting*, 1974, pp. 13–22.

[14] G. Berger and M. Goldman, "Comparison between some characteristic features of the positive electrical discharges for long and short air gaps," in *Proc. IEEE-PES Summer Meeting*, 1974, pp. 84–86.

[15] I. Gallimberti, "A computer model for streamer propagation," *J. Phys. D, Appl. Phys.*, vol. 5, pp. 2179–2189, 1972.

[16] M. Rizvi and J. Lovetri, "ESD source modeling in FDTD," in *Proc. IEEE Int. Symp. Electromagnetic Compatibility*, Chicago, IL, Aug. 22–27, 1994, pp. 77–82.

[17] P. F. Wilson and M. T. Ma, "Fields radiated by electrostatic discharges," *IEEE Trans. Electromagn. Compat.*, vol. 33, pp. 10–18, Feb. 1991.

[18] M. Angeli and E. Cardelli, "Numerical modeling of electromagnetic fields generated by electrostatic discharges," *IEEE Trans. Magn.*, vol. 33, pp. 2199–2202, Mar. 1997.

[19] P. M. McKenna, T. H. Rudolph, and R. A. Perala, "A time domain representation of the surface and transfer impedances useful for the analysis of advanced composite aircraft," in *Proc. Int. Aerospace and Ground Conf. Lightning and Static Electricity*, Orlando, FL, June 26–28, 1984.

Francescaromana Maradei (M'93) was born in 1969. She received the Laurea degree in electrical engineering (*cum laude*) from the University of Rome "La Sapienza," Rome, Italy, in 1992, the Diplome d'Etudes Approfondies (DEA) in electrical engineering from the Laboratoire d'Electrotechnique de Grenoble, Institut National Polytecnique de Grenoble, Grenoble, France, in 1993, and the Ph.D. degree in electrical engineering from the University of Rome "La Sapienza " in 1997.

In 1996, she joined the Department of Electrical Engineering, University of Rome "La Sapienza," where she is currently an Associate Professor. Her main interests are in numerical techniques and their application to EMC problems (shielding and transmission line analysis).

Prof. Maradei served as an Associate Editor of the IEEE Transactions on Electromagnetic Compatibility from 1999 to 2000. Since 1998, she has been a member of the Editorial Board of the IEEE Conference on Electromagnetic Field Computation (CEFC) and of the IEEE COMPUMAG Conference. She received the Oral Presentation Best Paper Award at the International Symposium on Electromagnetic Compatibility—EMC ROMA 1994, Rome, Italy, and the Poster Presentation Best Paper Award at the International Symposium on Electromagnetic Compatibility—EMC EUROPE 2000, Brugge, Belgium.

Marco Raugi was born in Livorno, Italy, in 1960. He received the degree in electronic engineering and the Ph.D. degree in electrical engineering from the University of Pisa, Pisa, Italy, in 1985 and 1990, respectively.

In 1990, he joined the Department of Electrical Systems and Automation, University of Pisa, where he is currently a Full Professor of Electrical Engineering. His main research interests are in the numerical computation of electromagnetic fields in nonlinear media and transmission lines.